

# Near field behavior of SnO<sub>2</sub> particle-layer deposited on standard optical fiber by electrostatic spray pyrolysis method

A. Cusano, P. Pilla, M. Consales, M. Pisco and A. Cutolo

Optoelectronic Division - Engineering Department - University of Sannio, Corso Garibaldi 107, 82100 Benevento, Italy.

[a.cusano@unisannio.it](mailto:a.cusano@unisannio.it)

A. Buosciolo

Department of Materials Engineering and Production, University of Naples "Federico II", P.le Tecchio 80, 80125 Napoli, Italy

M. Giordano

Institute for Composite and Biomedical Materials, National Research Council (IMCB-CNR), P.le Enrico Fermi 1, 80055 Portici, Italy

[gmichele@unina.it](mailto:gmichele@unina.it)

**Abstract:** We report the emergent optical near field profiles from standard single mode optical fibers on the cleaved end of which were deposited particle layers of SnO<sub>2</sub>. The layers, composed of micron and sub-micron sized particles, were deposited by means of Electrostatic Spray Pyrolysis (ESP) technique. Powerful analytical tools such as Atomic Force Microscopy (AFM) and Scanning Near-field Optical Microscopy (SNOM) were used to obtain simultaneously the SnO<sub>2</sub> layers topography and the related optical near field intensity distribution, when the fiber-substrate is illuminated by a light radiation in NIR range. We show that isolated microstructures, positioned in correspondence of the fiber core, reveal highly unusual capability of locally enhancing the collected optical near field. The observed phenomenon leads to new concepts of fiber optic chemical sensors and in fiber microsystems as well.

© 2006 Optical Society of America

**OCIS codes:** (180.5810) Scanning microscopy; (310.1860) Deposition and fabrication; (230.3990) Microstructure devices; (060.2370) Fiber optics sensors.

## References and links

1. K. Ishiguro, T. Sasaki, T. Arai, and I. Imai, "Optical and electrical properties of tin oxide films," *J. Phys. Soc. Jpn.* **13**, 296 (1958).
2. T. Seiyama, K. Fueki, J. Shiokawa, and S. Suzuki, "Chemical sensors," in *Proceedings of the International Meeting on Chemical Sensors*, K. Tokyo, Jpn ed.), (Elsevier, Amsterdam, 1983).
3. M. Batzill and U. Diebold, "The surface and materials science of tin oxide," *Prog. Surf. Sci.* **79**, 47-154 (2005).
4. M. Pisco, M. Consales, R. Viter, V. Smyntyna, M. Giordano, S. Campopiano, A. Cutolo, and A. Cusano, "Optoelectronic sensor for ammonia detection in water based on SnO<sub>2</sub> films as sensitive layer," *Proceedings of the First International Conference on Sensing Technology*, pp. 359-364 (2005).
5. A. Cusano, M. Consales, M. Pisco, P. Pilla, A. Cutolo, A. Buosciolo, R. Viter, V. Smyntyna and M. Giordano "Opto-chemical sensor for water monitoring based on SnO<sub>2</sub> particle layer deposited onto optical fibers by the electrostatic spray pyrolysis method," *Appl. Phys. Lett.* (to be published).
6. M. Pisco, M. Consales, S. Campopiano, R. Viter, V. Smyntyna, M. Giordano and A. Cusano "A novel opto-chemical sensor based on SnO<sub>2</sub> sensitive thin film for ppm ammonia detection in liquid environment," *J. of Lightwave Technol.* (to be published).
7. T. W. Ebbesen, H. J. Lezec, H. F. Ghaemi, T. Thio and P. A. Wolff, "Extraordinary optical transmission through sub-wavelength hole arrays," *Nature (London)* **391**, 667-669 (1998).
8. H. J. Lezec and T. Thio, "Diffracted evanescent wave model for enhanced and suppressed optical transmission through subwavelength hole arrays," *Opt. Express* **12**, 3629-3651 (2004).

9. R. Quidant, G. Badenes, S. Cheylan, R. Alcubilla, J.-C. Weeber, and C. Girard, "Sub-wavelength patterning of the optical near-field," *Opt. Express* **12**, 282-287 (2004).
10. E. H. A. Diagne and M. Lumbreras, "Elaboration and characterization of tin oxide-lanthanum oxide mixed layers prepared by the electrostatic spray pyrolysis technique," *Sens. Act. B* **78**, 98-105 (2001).
11. Y. Higashiyama, S. Tanaka, T. Sugimoto, and K. Asano, "Size distribution of the charged droplets in an axisymmetric shower," *J. of Electrostat.* **47**, 183-195 (1999).
12. Y. Matsui, M. Mitsuhashi, and Y. Goto, "Early stage of tin oxide film growth in chemical vapor deposition," *Surf. Coat. Technol.* **169**, 549-552 (2003).
13. A. Cusano, M. Pisco, M. Consales, S. Campopiano, A. Cutolo, R. Viter, V. Smyntyna, and M. Giordano, "Ammonia detection in water with a tin dioxide-based optical sensor," in *Optical Fibers: Applications*, L. R. Jaroszewicz, B. Culshaw, A. G. Mignani, eds., *Proc. SPIE* **5952**, 595214 (2005).
14. G. Binnig, C. F. Quate and C. Gerber, "Atomic force microscope," *Phys. Rev. Lett.* **56**, 930-933 (1986).
15. D. W. Pohl, W. Denk and M. Lanz, "Optical stethoscopy: Image recording with resolution  $\lambda/20$ ," *Appl. Phys. Lett.* **44**, 651-653 (1984).
16. Y. Eisenstein, T. Mokari, and U. Banin, "Fluorescence quantum yield of CdSe/ZnS nanocrystals investigated by correlated atomic-force and single-particle fluorescence microscopy," *Appl. Phys. Lett.* **80**, 4033-4035 (2002).
17. J. Prikulis, H. Xu, L. Gunnarsson, M. Kall and H. Olin, "Phase-sensitive near-field imaging of metal nanoparticles," *J. Appl. Phys.* **92**, 6211-6214 (2002).
18. U. Ben-Ami, N. Tessler, N. Ben-Ami, R. Nagar, G. Fish, K. Lieberman, G. Eisenstein, A. Lewis, J. M. Nielsen and A. Moeller-Larsen, "Near-Infrared contact mode collection near-field optical and normal force microscopy of modulated multiple quantum well lasers," *Appl. Phys. Lett.* **68**, 2337-2339 (1996).
19. J. J. Greffet and R. Carminati "Image formation in near field optics," *Prog. Surf. Sci.* **56**, 113-237 (1997).
20. M. Giordano, M. Russo, A. Cusano, A. Cutolo, G. Mensitieri, and L. Nicolais, "Optical sensor based on ultrathin films of  $\delta$ -form syndiotactic polystyrene for fast and high resolution detection of chloroform," *Appl. Phys. Lett.* **85**, 5349-5351 (2004).

## 1. Introduction

SnO<sub>2</sub> belongs to the important family of oxides whose extremely wide range of physical and chemical properties makes them exciting materials for basic research and for technological applications alike [1]. Solid state gas sensors is a field in which they play a dominant role. A wide variety of oxides exhibit sensitivity towards oxidizing and reducing gases by a variation of their electrical properties, but SnO<sub>2</sub> was one of the first considered material for these applications, and it is still the most frequently used [2]. The sensing mechanism of SnO<sub>2</sub>-based sensors is founded on electrical conductance change upon surface reduction oxidation (redox) reactions with gas species. Since only the surface layer is affected by the reaction, the sensitivity increases for a decreasing thickness, thus motivating the development of thin film metal oxide sensors. The main disadvantage of SnO<sub>2</sub>-based sensors is that they require a very high operating temperature (250-450°C) to enhance redox reactions so as to achieve the optimum sensitivity. Up to now, because of their principles of operation and high operating temperatures, the common SnO<sub>2</sub>-based resistive sensors have never been employed in liquid environments [3]. In our recent works, we demonstrated the possibility to use SnO<sub>2</sub> as sensitive layer for fiber optic chemical sensors. They are able to work at room temperature and in liquid environment exploiting all the advantages of an optical transducing technique [4, 5, 6]. To the aim, thin films of SnO<sub>2</sub> have been deposited by the Electrostatic Spray Pyrolysis (ESP) method onto single-mode silica optical fiber cleaved end. The excellent sensor sensitivity, good recovery features, high repeatability and fast response times, suggested the investigation of the surface and interface properties of the deposited SnO<sub>2</sub> layers. In fact, it was observed that the best performances were obtained with particle layer films exhibiting surface rugosity approaching the optical wavelength and able to significantly modify the local near field [5]. Based on these preliminary observations, the present work is aimed to find the physical explanations for the surprising sensitivity of SnO<sub>2</sub> particle layers based optical sensors. In particular, here, we report on the highly unusual capability of isolated SnO<sub>2</sub> microstructures of locally enhancing the emergent optical near field profiles from single mode optical fibers. For this purpose, a complex equipment constituted by simultaneous AFM (Atomic Force Microscopy) and SNOM (Scanning Near Field Optical Microscopy) techniques was used to correlate samples morphology and optical behavior. This study reveals an unusual capability of particle layer films to manipulate light, which is of great interest in various application fields ranging from high density data storage to optical circuitry and also

for optical trapping and sensing. However, the path toward the miniaturization of photonic circuits to the nanoscale has the diffraction limit on its way.

In recent years many attempts to circumvent this limit have been done. Ebbsen et al. [7] described an experiment in which they showed light through a periodic array of nano-holes in a silver film. They reported on an enhanced transmission of light at wavelengths bigger than the period of the array. However, it has been demonstrated [8] that enhanced transmission through sub-wavelength hole arrays can be obtained also by non-metallic systems by interference of diffracted evanescent waves. To achieve a non-diffraction limited light confinement Quidant et al. [9] proposed a regular array of gold nano-particles on a dielectric substrate which is able, under appropriate illumination conditions, to pattern the optical near field giving rise to subwavelength light spots between the structures.

The phenomenon we observed opens the way to the manipulation of light through metal oxide micro and nano sized structures; in fact, by finding the appropriate process parameters for the ESP deposition or acting a posteriori by laser micromachining, it would be possible to obtain the desired structures onto the core of the optical fiber, in order to concentrate the total emerging field in precise localized spots.

## 2. Materials and methods

### 2.1 ESP deposition technique

Spray pyrolysis methods have been used to fabricate porous-ceramic-layers composed by micron and submicron-sized particles [3]. Among them, the Electrostatic Spray Pyrolysis (ESP) method has been newly developed in this decade and it has resulted advantageous in terms of facility to produce uniform particles, simplicity of ambient atmospheric apparatuses and selectivity of inexpensive and harmless solvents such as water or ethanol. In addition it allows to change the film features, such as porosity, thickness, roughness, etc, by changing the deposition parameters and conditions [10].

We used ESP technique to deposit an SnO<sub>2</sub> particle layer onto the distal end of standard single mode optical fibers working in the NIR range. For a detailed description of the deposition technique we remand to the cited articles [10, 11]. For the sample fabrication, an ethanol solution of SnCl<sub>4</sub>·5H<sub>2</sub>O was inserted in a syringe connected with a metallic needle. Fibers heads were located in a grounded metal substrate, which integrates a resistive heater supplied of a chromium-nickel thermocouple for the temperature monitoring. A high electric field was applied between the syringe needle and the grounded metal substrate by means of a high voltage source. This deposition method is based on the phenomenon of polarization of electrolyte (usually ethanol or water solutions of metal chlorides) on charged droplets by electrostatic field. The polarized droplets of the solution are separated by repulsive forces and are carried by electrostatic field along its force lines [11]. When the droplets reach the heated substrate, chemical reaction of tin chloride with water vapor of solution, stimulated by the temperature, takes place providing the formation of the tin dioxide film [12]:



The deposition temperature was 320±5°C and the liquid flow kept constant at 0.37ml/min. by means of an air pump. Further deposition parameters will be specified later during the description of each sample. The deposited layers were preliminary investigated by elemental analysis and SEM images [13]. Experimental results revealed a complete and homogeneous coverage of the fiber core surface (approx. 500 nm from spectral measurements). Furthermore, SEM images were not able to resolve the surface roughness as revealed by preliminary measurements carried out by AFM/SNOM technique [5].

### 2.2 AFM/SNOM set-up

Scanning probe techniques were used in order to have quantitative information of the surface structures and knowledge of the relationship between the layer morphology and the optical near field. AFM and SNOM techniques [14, 15] are emerging as powerful analytical tools

enabling sub-wavelength spatial resolution and appreciation of optical properties and structures in the mesoscale [16, 17].

Our apparatus, showed in Fig. 1. is an AFM/SNOM system capable of simultaneous collection mode SNOM and normal force AFM imaging using the same tip.

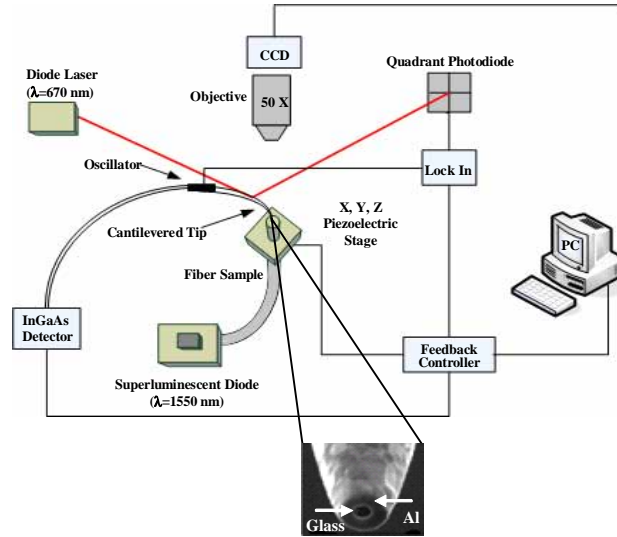


Fig. 1. AFM/SNOM experimental set up (direct configuration).

This equipment is characterized essentially by high  $z$  sensitivity, high stability against vibrations, and low thermal drift. A 3D flat scanner allows up to 75 microns of  $x$ ,  $y$  and  $z$  fine motion of the sample and a high resolution in the  $z$  direction  $\approx 0.01$  nm. Normal force sensing is accomplished by readily reflecting a diode laser beam off the cantilever onto a position-sensitive detector. Cantilevered near-field optical probe, prepared from tapered optical fibers, can easily fit under the lens of a conventional microscope since the sub-wavelength tip is only 50 microns from the point at which the fiber is cantilevered. This permits a high numerical aperture lens to be brought close to the sample allowing to target the scanning area. A CCD is employed to guide effectively the tip to the core region of the fiber by a far-field optical objective. This is the only SPM system able to perform perpendicular nanometric alignment of the tip on the fiber sample [18]. The light injected into the fiber sample can be collected by SNOM probe that scanning the surface, produces an image of the emergent optical near field intensity.

The  $\text{SnO}_2$  treated fibers, were coupled to a superluminescent diode with central wavelength  $\lambda=1550$  nm and an output power  $\approx 0.25$  mW; the emergent optical field from the layer was then collected by the SNOM tip which was in turn coupled to an InGaAs detector. By scanning the sample, we were able to reconstruct simultaneously the topography of the  $\text{SnO}_2$  layer and the related intensity distribution of the emergent optical near field. The images were obtained in “constant-amplitude” mode, with the normal force feedback loop to maintain constant tip distance from the surface.

### 3. Results and discussion

We report the results relative to four samples, labelled  $a$ ,  $b$ ,  $c$  and  $d$  respectively, that revealed the most interesting features. All the images were taken in a region approximately centered on the core of the optical fiber illuminated by the superluminescent diode; moreover all the

images were obtained by using the same SNOM probe (Cr-Au coated multimode fiber 200-1200 nm) with aperture diameter  $d=300$  nm.

SNOM images resolution is limited by the size of the probe aperture (diameter  $d=300$  nm). AFM images resolution in the  $x, y$  directions is of the order of the probe terminal part dimension (aperture diameter plus the metallization layer  $\approx 450$  nm), otherwise in  $z$  direction, the limit is given by piezoelectric precision: when the minimum scan range of the flat scanner is set ( $1.5 \mu\text{m}$  range) it corresponds to about  $0.01$  nm; when middle scan range ( $5 \mu\text{m}$  range) is set it is about  $0.1$  nm.

### 3.1 Flat $\text{SnO}_2$ film

In Fig. 2(a), we report a 3D image of the sample *a* topography obtained using a solution volume of  $5$  ml, a concentration of  $0.01$  mol/l and a deposition time  $2' 10''$ . The image refers to a  $(13 \times 13) \mu\text{m}$  area, approximately centered on the optical fiber core, indicated with a red circle; this image reveals that the deposited layer is very flat with an average surface height histogram of about  $40.0$  nm. From Fig. 2(b), it is possible to note that the optical near field collected on the sample surface, simultaneously to its topography, is not influenced by the presence of the  $\text{SnO}_2$  layer, in fact it has the expected Gaussian profile of the emergent field from the cleaved end of a single mode optical fiber.

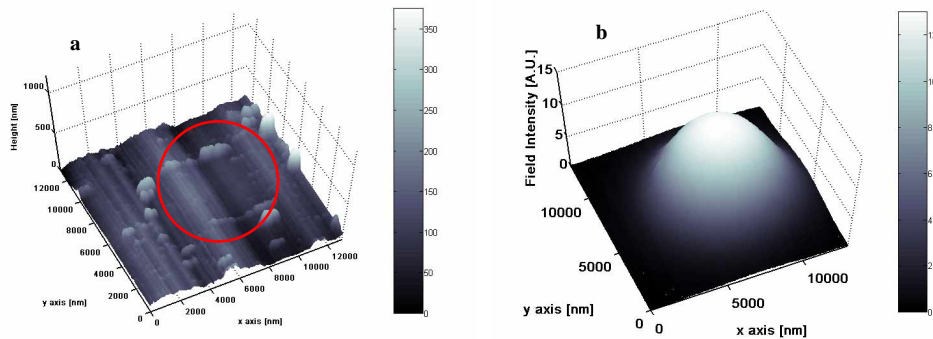


Fig. 2. Topographic image of the sample *a*, in which is showed the core region with the red circle (a) and optical near field simultaneously collected by the SNOM probe in the same region  $(13 \times 13) \mu\text{m}$  (b).

### 3.2 High roughness $\text{SnO}_2$ film

In Fig. 3(a), we report a 3D image of the sample *b* topography obtained using a solution volume of  $5$  ml, a concentration of  $0.01$  mol/l and a deposition time  $2' 20''$ . The image refers to a  $(13 \times 13) \mu\text{m}$  area, centered on the optical fiber core. It reveals the presence of several  $\text{SnO}_2$  bumps. In order to obtain quantitative information about the sample topography we analyzed the distribution of the bumps heights and sizes in the image. From the heights histogram, relative to the core region of the image, we revealed that the mean height is about  $410.6$  nm and the standard deviation is about  $126.3$  nm, as reported in Fig. 4(a). The distribution of bumps size revealed the presence of about  $183$   $\text{SnO}_2$  bumps, covering about  $14\%$  of the total area, as reported in Fig. 4(b). Supposing the bumps have a circular base, from the mean area it is possible to derive the mean radius and so the mean lateral dimension:  $\bar{x} \approx \bar{y} \approx 465$  nm. Figure 3(b), demonstrates that in correspondence of the biggest bumps there is a light diffraction effect and thus a modification of the near field profile transmitted through the optical fiber coating.

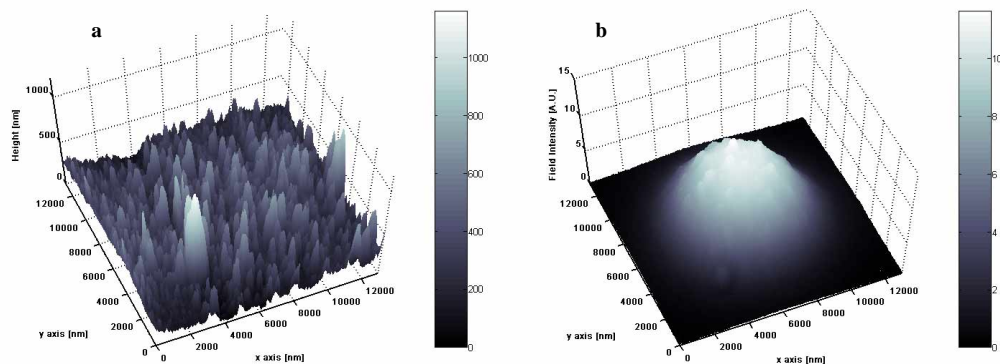


Fig. 3. Topographic image of the sample *b* (a) and optical near field simultaneously collected by the SNOM probe in the same region (13x13)  $\mu\text{m}$  (b).

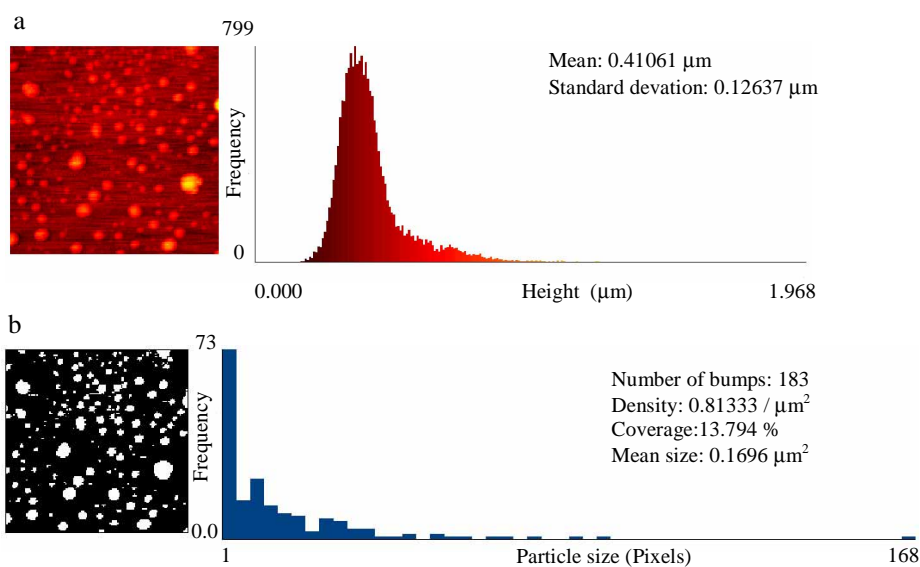


Fig. 4. Histogram of the heights relative to a squared region strictly containing the core region of the sample *b* (a) and analysis of bumps present in the same region (b).

In this case, the bumps have a mean height of about 700 nm and a mean width of about 550 nm. In fact, it can be clearly observed how the typical Gaussian shape of the fundamental mode propagating through the single-mode optical fiber is modified in correspondence of these  $\text{SnO}_2$  peaks. This can be justified by considering the high refractive index of the  $\text{SnO}_2$  (approx. 1.967 at  $\lambda=1550$  nm) bumps which in turn try to guide the light. However, the lateral dimensions and the bumps spacing (mean bumps spacing is about 1  $\mu\text{m}$ ) are too small to allow a correct light localization due to the significant overlap of the evanescent field. This interpretation was also confirmed by additional experiments reported in the following and

focused on the investigation of the particle layer effects in the case of larger and isolated particles.

### 3.3 Dual structure SnO<sub>2</sub> film

In Fig. 5(a), we report a 3D image of the sample *c* topography obtained using a solution volume 5 ml, a concentration of 0.001 mol/l and a deposition time 2' 10". The image refers to a (6x6) μm area, centered on the optical fiber core; it reveals the presence of two SnO<sub>2</sub> peaks very close to each other and not perfectly resolved because the tip is too large compared to the spatial separation between the structures. The characteristic dimensions of the two structures are:  $x_1 \approx 1700$  nm,  $y_1 \approx 2700$  nm,  $z_1 \approx 2600.0$  nm and  $x_2 \approx 1300$  nm,  $y_2 \approx 1900$  nm,  $z_2 \approx 2100.0$  nm.

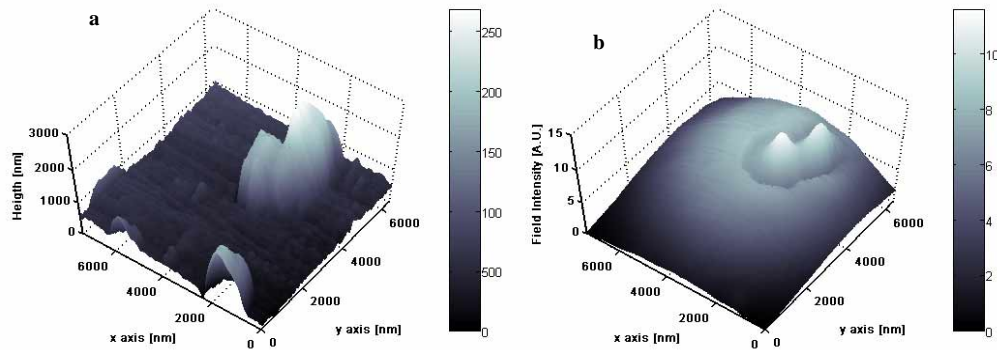


Fig. 5. Topographic image of the sample *c* (a) and optical near field simultaneously collected by the SNOM probe in the same region (6x6) μm (b).

Figure 5(b). demonstrates that the presence of the two microstructures, with dimensions comparable to the wavelength of the radiation, leads to a surprisingly modification of near field profile transmitted through the optical fiber coating: the optical near field is locally enhanced in correspondence of these microstructures. In this case, the lateral dimensions and the structures spacing (that is about 1.4 μm) are able to confine light in the high refractive index SnO<sub>2</sub> structures leading to an effective light localization.

### 3.4 Single structure SnO<sub>2</sub> film

The most pronounced effect of the optical near field enhancement was observed for the sample *d* (prepared using the same deposition parameters of the sample *c*), whose topography is characterized by the presence of an isolated microstructure in the fiber core region, as shown in Fig. 6(a). The isolated microstructure has approximately the shape of an half ellipsoid, with dimensions  $x \approx 1800$  nm,  $y \approx 2100$  nm and  $z \approx 2500.0$  nm, on a flat SnO<sub>2</sub> substrate. It is evident from Fig. 6(b). that the optical near-field is strongly enhanced in correspondence of the microstructure.

Before discussing the obtained results, we want to stress, once again, that the optical images showed represent the collected optical near field intensity distribution emitted by a standard optical fiber with an SnO<sub>2</sub> coating, when it is illuminated by a superluminescent diode. In other words, they don't represent a contrast due to intrinsic optical properties of the sample. Hence the strong correlation between samples topography (*b*, *c* and *d*) and near field profiles reveal an effective enhancement of the optical near field in correspondence of the structures and it is not a contrast enhancement between a flat substrate and particles with different dielectric constant respect to the substrate [19]. This was also supported by the experimental evidence that flat SnO<sub>2</sub> films were not able to influence the optical near field

emerging from a single mode fiber. On the contrary, a different behavior was observed in the case of particle layer films characterized by the presence of structures with dimensions comparable to the operating wavelength injected into the fiber itself.

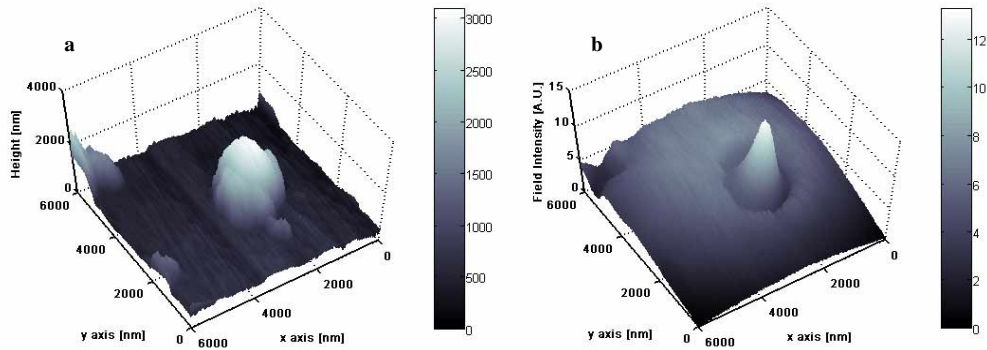


Fig. 6. Topographic image of the sample *d* (a) and optical near field simultaneously collected by the SNOM probe in the same region (6x6)  $\mu\text{m}$  (b).

Moreover, in order to demonstrate that the field enhancement is observable only in the near field range, we also recorded the emergent field at a constant sample-probe distance of approximately 2  $\mu\text{m}$  as reported in Fig. 7. For a sample-tip distance comparable to the optical wavelength, the field profile is not able to completely maintain information about the film morphology, even if a significant distortion of the beam shape is still clearly observable. By increasing the sample-tip distance, up to few times the wavelength (we selected 7  $\mu\text{m}$ ), the collected optical field profile assumes the Gaussian shape, as expected in far field imaging.

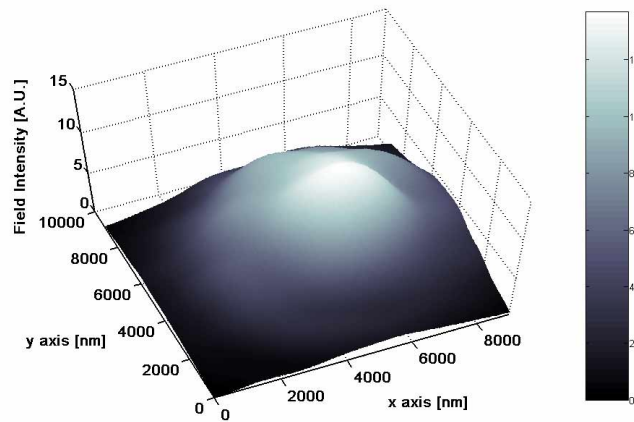


Fig. 7. Emergent field collected from the sample *d* at constant sample-tip distance of about 2  $\mu\text{m}$ .

With regard to the sample *d*, if we suppose that the optical field perturbation is only local (in correspondence of the microstructure), then the unperturbed field can be obtained by

interpolating the data upon the exclusion of the microstructure related area. We found that the integrals of the intensity of the perturbed and unperturbed optical field respectively are equal, inferring that the microstructure produces a local redistribution of the intensity distribution. In Fig. 8, we reported a cross-section of the measured intensity distribution (solid line) and of the interpolating surface (dotted line) obtained as described above. The local intensity enhancement, calculated as the ratio between the maximum measured intensity and the corresponding intensity of the unperturbed field is about 1.8. The spot-size of the enhanced field measured at FWHM (Full Width Half Maximum) is about 500 nm.

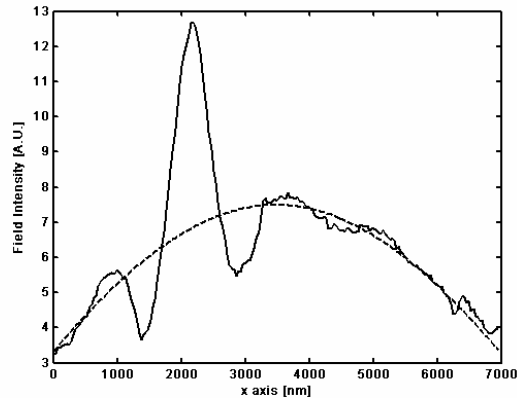


Fig. 8. A cross-section of the measured intensity of the optical near field (solid line) emergent from the sample *d*, relative to a line parallel to the *y* axis of the figure 6 (b) passing through the peak and of the interpolating surface (dotted line).

In order to better understand the nature of the local field enhancement an additional test was carried out. We modified the experimental set-up, described in section 2.2, as follows: the cantilevered optical probe was coupled to the superluminescent diode and the fiber sample was coupled to the InGaAs detector while all the other components were the same (Fig. 9).

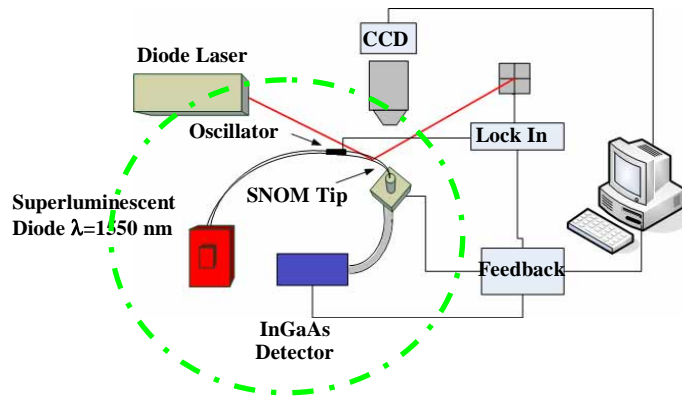


Fig. 9. Reverse experimental set up.

In this way, by scanning the SNOM probe on the sample surface (in a region approximately centered onto the fiber core), it was possible to construct a map of the radiation intensity

coupled into the standard optical fiber coated with the  $\text{SnO}_2$  overlay. Figure 10. shows that the profile of the radiation intensity coupled to the sample fiber using the reverse configuration, is very similar to that one transmitted through the optical fiber coating and collected in the forward configuration. In this case the local intensity enhancement is about 1.5 calculated using the same procedure reported above in the text.

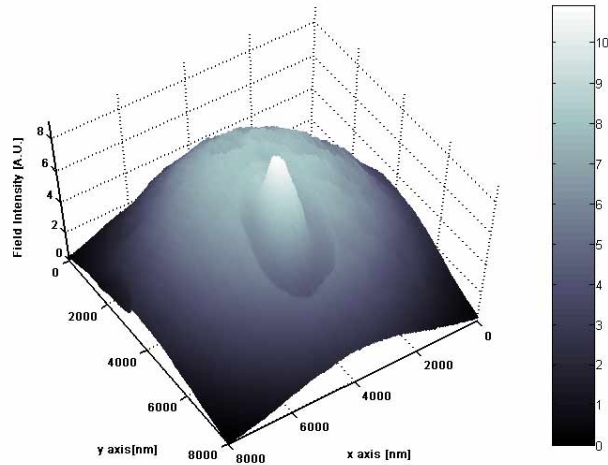


Fig. 10. The radiation intensity coupled into the standard optical fiber when it was illuminated by the SNOM probe.

Based on these results, it is possible to give an effective explanation of the observed phenomenon. Referring to the direct configuration, we can say that the radiation impinging at the base of the microstructure, coming from the layer of the same material, continues to propagate inside of it confined by the high refractive index contrast between the oxide ( $\text{SnO}_2$  refractive index: 1.967 for  $\lambda=1550$  nm, as above reported) and the air and by the geometry of the microstructure. Near the structure surface and its end, part of the propagative field becomes evanescent and it will be detected by the SNOM probe together with the propagative one. It is well known that when focusing a light beam into a sub-wavelength spot, the electric field of such spot may be represented as the sum of propagating and evanescent modes. In near-field zone the contribution of evanescent modes may become significant compared to propagating modes. Inversely in far-field zone only the propagating modes may be considered. In other words, the local enhancement of the optical field in the region of the microstructure is also accompanied by a conversion of part of the field from propagative to evanescent. We collected radiation in the near-field zone by the cantilevered optical probe thus recording the sum of the two contributions. Since the structure dimensions are comparable to the radiation wavelength (as revealed from AFM measurements) we can exclude that the local field enhancement can be due to truly evanescent field. In addition, the reverse profile is very similar to that one obtained in forward configuration indicating a strong reciprocity not compatible with a structure able to convert at its ends (due to diffraction limit) all the propagating contribute in the evanescent counterpart.

We can conclude that the particle-layer acts as an element able to guide and focus light and that it works in both direct and reverse configuration.

### 3.5 Discussion

The phenomenon that we have observed gives an explanation of the surprising high sensitivity exhibited by  $\text{SnO}_2$  based fiber optic sensors. As matter of fact, when working with fiber optic

chemical sensors based on the deposition of a sensitive layer onto the cleaved end of the fiber, it is usual to schematize the layer as a Fabry Perot interferometer having a uniform thickness on the core region so that the reflectivity at the interface fiber-layer can be obtained by the sum of multiple reflections [20]. However, for structured films the surface exhibits microstructures able to strongly perturb the emergent optical field profile producing its local enhancement and focusing. In this case, the interaction of the field with the analyte occurs not in the volume of the sensitive layer but mainly on its surface by means of the evanescent part of the field (this is confirmed by the fact that the light is so squeezed by the structure that the part of evanescent wave should be greatly enhanced). This can improve the performances of fiber optic sensors based on metal oxides since they rely mainly on surfaces interactions. In addition, a sensing mechanism based on surface interactions is also advantageous in terms of sensor response times, since no diffusion of the analyte in the volume of the sensitive layer is needed. Further studies to better understand the effects of the film topography, and thus of the field profile, on the optical fiber sensors sensitivity are currently on going.

Concerning the possible applications in the field of in-fiber micro systems, it is important to deposit the microstructures in a controlled way. This becomes possible finding the appropriate process parameters for the ESP deposition or acting a posteriori by laser micromachining; in this way, it is obtained a concentration of the total emerging field in different localized spots. In addition, the interference of diffracted evanescent waves, generated by the focusing of the field in sub-wavelength areas, could give place to other localized spot of field in between the microstructures, thus acting as a photonic bandgap crystal.

#### **4. Conclusion**

In conclusion, we reported about the morphological and optical behavior of SnO<sub>2</sub> particle layers deposited with a very simple deposition technique such as the ESP, on the cleaved end of a standard single mode optical fibers. The characterization of the particle layers were carried out by means of a very powerful tool such as an AFM/SNOM apparatus capable of sub-wavelength spatial resolution. The particular morphological structures found on the core of the fibers showed an unusual capability of locally enhance the optical near field. The near field collected in presence of SnO<sub>2</sub> layers with a flat surface and a mean of the surface height histogram of the order of tens of nanometers, showed the typical Gaussian shape of the fundamental mode propagating through the single-mode optical fiber. In presence of layers characterized by several SnO<sub>2</sub> bumps, with mean lateral dimensions of about 550 nm and a mean height of about 700 nm, the near field profile resulted to be modified in correspondence of them; however, the lateral dimensions and the bumps' spacing are too small to allow a correct light localization due to the significant overlap of the evanescent field. Finally the near field corresponding to layers characterized by the presence of isolated microstructures revealed high capability of light localizations and focusing combined with a strong increasing of the evanescent wave content. This effect is the main feature able to provide the high sensitivity to surface interactions due to chemical sorption experimentally observed. Further investigations will be focused on the validation of our work by a direct correlation between sensing performances, morphological and near field optical behavior. Finally, great effort will be also devoted to the optimization of the deposition process especially in terms of controllability and repeatability of the realized particle layer films.